

Weak gravitational lensing as a probe of physical properties of substructures in dark matter halos

Masato Shirasaki

Department of Physics, University of Tokyo, Tokyo 113-0033, Japan

masato.shirasaki@utap.phys.s.u-tokyo.ac.jp

ABSTRACT

We propose a novel method to select satellite galaxies in outer regions of galaxy groups or clusters using weak gravitational lensing. The method is based on the theoretical expectation that the tangential shear pattern around satellite galaxies would appear with negative values at an offset distance from the center of the main halo. We can thus locate the satellite galaxies *statistically* with an offset distance of several lensing smoothing scales by using the standard reconstruction of surface mass density maps from weak lensing observation. We test the idea using high-resolution cosmological simulations. We show that subhalos separated from the center of the host halo are successfully located even *without* assuming the position of the center. For a number of such subhalos, the characteristic mass and offset length can be also estimated on a statistical basis. We perform a Fisher analysis to show how well upcoming weak lensing surveys can constrain the mass density profile of satellite galaxies. In the case of the Large Synoptic Survey Telescope with a sky coverage of $20,000 \text{ deg}^2$, the mass of the member galaxies in the outer region of galaxy clusters can be constrained with an accuracy of ~ 0.1 dex for galaxy clusters with mass $10^{14} h^{-1} M_{\odot}$ at $z = 0.15$. Finally we explore the detectability of tidal stripping features for subhalos having a wide range of masses of $10^{11} - 10^{13} h^{-1} M_{\odot}$.

1. INTRODUCTION

The standard Λ CDM cosmology was established by an array of recent observations such as the cosmic microwave background (CMB) anisotropies (e.g., Komatsu et al. 2011; Hinshaw et al. 2013) and the large-scale structure of the universe (e.g., Tegmark et al. 2006; Reid et al. 2010). A generic prediction of the Λ CDM model is that structure grows hierarchically, with smaller dark matter halos forming first and then merging to form larger halos through various processes including accretion, stripping and mergers. In order to study the nonlinear structure growth observationally, it is essential to probe the dark matter distribution in massive dark halos. Gravitational lensing provides a powerful method to probe matter distribution. Small image distortions of distant galaxies are caused by the foreground gravitational field. The small distortion is called cosmic shear and contains, in principle, rich information about the matter distribution at small and large scales.

Previous studies extensively utilized gravitational lensing observations, but mainly focused on some specific objects such as individual galaxy clusters where dark matter contribute most of the mass. It is still difficult to measure the mass distribution of individual isolated galaxies. However, one can measure the average cosmic shear signals across a large sample as a function of angular separation with a high significance level. The so-called galaxy–galaxy lensing has been applied to various gravitational lensing observations (e.g., Brainerd et al. 1996; Hudson et al. 1998; Guzik & Seljak 2002; Hoekstra et al. 2004; Mandelbaum et al. 2006b; Gillis et al. 2013; Velander et al. 2014). For galaxy clusters, the large-scale cosmic shear can be measured in a similar statistical manner (e.g., Mandelbaum et al. 2006a; Johnston et al. 2007; Okabe et al. 2013; Covone et al. 2014) or on individual basis (e.g., Broadhurst et al. 2005; Hamana et al. 2009; Oguri et al. 2012; Okabe et al. 2014). Such measurements clearly show that the total matter distribution around isolated galaxies and galaxy clusters can be well described by the so-called NFW profile (Navarro et al. 1997).

In a hierarchical universe, it is expected that nonlinear halos contain rich substructures that probably host satellite galaxies. When small halos fall into a larger host halo, they would suffer tidal effects from the host halo, such as tidal stripping and impulsive heating. Some subhalos may survive such interactions and are likely to host member galaxies in galaxy clusters at the present time. Therefore, studying the matter distribution around subhalos in nonlinear halos is important and serves as a fundamental test of hierarchical structure formation.

Unfortunately, measuring the mass distribution around subhalos is a substantially more difficult task than for isolated galaxies and galaxy clusters because the overall amplitude of the shear signal from subhalos is significantly smaller. The strong lensing effect is known to be a powerful probe of substructures (Kneib & Natarajan 2011), but one can use the method only to probe the central region of dark matter halos. Clearly, another technique is needed to probe substructures that reside in the outer region of dark matter halos.

There have been a few, limited studies that were aimed at extracting the shear signal by subhalos in galaxy clusters. One needs, however, a priori information on the radial distribution of the subhalos inside the host halo in order to separate the substructure contribution from the smoothed component of the host halo. For example, Li et al. (2014) use a group catalog constructed from the Sloan Digital Sky Surveys (SDSS) by the adoptive halo-based group finder of Yang et al. (2005, 2007). The group catalog generally contains the information of the radial distribution of member galaxies with respect to the position of the brightest galaxy in each galaxy-group halo. The authors generate subsamples utilizing the projected offset lengths of the member galaxies and measure the average cosmic shear signals for each subsample. Their result is broadly consistent with the theoretical expectation from hierarchical structure formation. However, it is assumed that the brightest galaxy is located at the center of the host halo. Li et al. (2014) discuss potential effects of off-centering on the measurement of the mass distribution around subhalos.

In this paper, we propose a novel method to locate and characterize subhalos. Since we can reconstruct surface-mass density observationally, we define the main halo centers as the maxima of

the surface-mass density in region of interest. Our method uses a smoothed lensing mass map. The tangential cosmic shear around subhalos has a negative value at the offset length from the center of each main halo. This interesting feature enables us to select the satellite galaxies in galaxy groups and clusters by measuring the smoothed tangential shear. Our method has the major advantage that the center of host halos does not need to be determined throughout the analysis.

The paper is organized as follows. In Section 2, we briefly describe the average cosmic shear signal obtained from galaxy–galaxy lensing analysis with the standard galaxy group catalogs. There, we explain the basic idea of our method of locating substructures away from the center of main host halo. In Section 3, we use a large set of N -body simulations to construct mock weak lensing maps and demonstrate the ability of our method. We then forecast constraining the matter density profile around the subhalos selected by our method in the upcoming wide field lensing surveys in Section 4. Conclusions and discussions are summarized in Section 5.

2. GALAXY–GALAXY LENSING

Galaxy–galaxy lensing provides a statistical method to probe the cross correlation between galaxy and matter

$$\xi_{\text{g,m}}(r) = \langle \delta_{\text{g}}(\mathbf{x}) \delta_{\text{m}}(\mathbf{x} + \mathbf{r}) \rangle, \quad (1)$$

where δ_{g} and δ_{m} are overdensities of galaxies and matter. The cross correlation is related to the projected surface-mass density

$$\Sigma(R) = 2\bar{\rho}_{\text{m}} \int_R^\infty \xi_{\text{g,m}}(r) \frac{r \, dr}{\sqrt{r^2 - R^2}}, \quad (2)$$

where $\bar{\rho}_{\text{m}}$ is the mean matter density of the universe. Galaxy–galaxy lensing measures the azimuthally averaged tangential shear of the background galaxies (sources) as a function of angular separation around a large set of the foreground galaxies (lenses). The observable $\gamma_t(R)$ is related to the excess surface matter density $\Delta\Sigma(R)$ as follows:

$$\gamma_t(R) = \frac{\Delta\Sigma(R)}{\Sigma_{\text{crit}}} = \frac{\bar{\Sigma}(R) - \Sigma(R)}{\Sigma_{\text{crit}}}, \quad (3)$$

where $\bar{\Sigma}(R)$ is given by

$$\bar{\Sigma}(R) = \frac{4\bar{\rho}_{\text{m}}}{R^2} \int_0^R y \, dy \int_y^\infty \xi_{\text{g,m}}(r) \frac{r \, dr}{\sqrt{r^2 - y^2}}. \quad (4)$$

Σ_{crit} is known as the critical density defined by the following relation

$$\Sigma_{\text{crit}} = \frac{c^2}{4\pi G} \frac{D_{\text{s}}}{D_1 D_{1\text{s}}}, \quad (5)$$

where D_{s} , D_1 , and $D_{1\text{s}}$ are the angular diameter distance to the source, the lens, and between the source and the lens, respectively.

2.1. Theoretical Model

Here, we describe the model of the lensing observable γ_t around galaxies. In what follows, we distinguish the lensing signal due to the central galaxies from that due to the satellite galaxies. In the present paper, we define the central galaxy as the brightest cluster galaxy (BCG). BCG is commonly used as a reference to the central galaxy in optical surveys of galaxies. Satellite galaxies are other member galaxies in a given group, except the central galaxy¹.

Central Galaxies

Central galaxies are expected to be located at the center of host halos. If a central galaxy is exactly located at the center, the lensing signal around it is dominated by the contribution from the smoothed matter distribution within the host halo at small angular scales. Let us suppose that the density profile of the host halo is described by the truncated NFW profile (Baltz et al. 2009),

$$\rho_h(r) = \frac{\rho_s}{(r/r_s)(1+r/r_s)^2} \left(\frac{r_t^2}{r^2 + r_t^2} \right)^2, \quad (6)$$

where ρ_s and r_s are the scale density and the scale radius, respectively. r_t in Equation (6) denotes the truncation radius. The parameters ρ_s and r_s can be essentially convolved into one parameter, the concentration $c_{\text{vir}}(M, z)$, by the use of two halo mass relations; namely, $M = 4\pi r_{\text{vir}}^3 \Delta_{\text{vir}}(z) \rho_{\text{crit}}(z)/3$, where r_{vir} is the virial radius corresponding to the overdensity criterion $\Delta_{\text{vir}}(z)$ (as shown in, e.g., Navarro et al. (1997)), and $M = \int dV \rho_h(\rho_s, r_s)$ with the integral performed out to r_{vir} . In this paper, we adopt the functional form of the concentration parameter in Duffy et al. (2008),

$$c_{\text{vir}}(M, z) = 5.72 \left(\frac{M}{10^{14} h^{-1} M_{\odot}} \right)^{-0.081} (1+z)^{-0.71}. \quad (7)$$

Oguri & Hamana (2011) study the lensing observable around dark matter halos in detail using a large set of numerical simulations. They show that the typical truncation radius is about two to three times the virial radius for halos with masses $5 \times 10^{13} - 5 \times 10^{14} h^{-1} M_{\odot}$. Throughout this paper, we assume $r_t = 2.6 r_{\text{vir}}$ as shown in Oguri & Hamana (2011). At small angular scales, one can calculate γ_t by replacing $\bar{\rho}_m \xi_{g,m}$ with ρ_h in Equation (3). In this case, γ_t is given by

$$\gamma_t(R) = \bar{\kappa}_h(R) - \kappa_h(R), \quad (8)$$

¹ In the present paper we do not consider that some satellite galaxies in a group may actually be hosted in another group halo along the line of sight. This contamination would induce the biased parameter estimation of subhalo properties. Li et al. (2013) estimate the impact of this contamination on galaxy-galaxy lensing analysis for satellite galaxies in a group by using mock galaxy catalogs. They show that $\sim 10\%$ of satellites would actually be hosted in another group. This 10% contamination would cause the biased estimation of the satellite mass with a level of $\sim 50\%$. However, one can correct this bias by an appropriate model taking into account the possibility of misidentification of satellites. The detail is found in Li et al. (2013).

where

$$\begin{aligned} \kappa_h(R) &= \frac{4\rho_s r_s}{\Sigma_{\text{crit}}} \frac{\tau}{4(\tau^2 + 1)^3} \left[\frac{2(\tau^2 + 1)}{x^2 - 1} \{1 - F(x)\} + 8F(x) + \frac{\tau^4 - 1}{\tau^2(\tau^2 + x^2)} \right. \\ &- \left. \frac{\pi [4(\tau^2 + x^2) + \tau^2 + 1]}{(\tau^2 + x^2)^{3/2}} + \frac{\tau^2(\tau^4 - 1) + (\tau^2 + x^2)(3\tau^4 - 6\tau^2 - 1)}{\tau^3(\tau^2 + x^2)^{3/2}} L(x) \right], \end{aligned} \quad (9)$$

$$\begin{aligned} \bar{\kappa}_h(R) &= \frac{4\rho_s r_s}{\Sigma_{\text{crit}}} \frac{\tau^4}{2(\tau^2 + 1)^3 x^2} \left[2(\tau^2 + 4x^2 - 3)F(x) + \frac{1}{\tau} \{ \pi(3\tau^2 - 1) + 2\tau(\tau^2 - 3) \ln \tau \} \right. \\ &+ \left. \frac{1}{\tau^3 \sqrt{\tau^2 + x^2}} \{ -\tau^3 \pi(4x^2 + 3\tau^2 - 1) + [2\tau^4(\tau^2 - 3) + x^3(3\tau^4 - 6\tau^2 - 1)] L(x) \} \right], \end{aligned} \quad (10)$$

where $x = R/r_s$ and $\tau = r_t/r_s$ and $F(x)$ and $L(x)$ are

$$F(x) = \begin{cases} \frac{1}{\sqrt{1-x^2}} \operatorname{arctanh} \sqrt{1-x^2} & (x < 1), \\ \frac{1}{\sqrt{x^2-1}} \operatorname{arctan} \sqrt{x^2-1} & (x > 1), \end{cases} \quad (11)$$

$$L(x) = \ln \left(\frac{x}{\tau + \sqrt{\tau^2 + x^2}} \right). \quad (12)$$

Off-centering Effect and Neighboring Halos

The position of the central galaxy may be offset from the center of the host halo. The off-centering of the central galaxies induces the effective smoothing effect of the observable γ_t in a galaxy–galaxy lensing analysis. We model this effect following Oguri & Takada (2011). The smoothing effect may be expressed by

$$\gamma_t(\theta) = \int \frac{\ell d\ell}{2\pi} \kappa_{M,\text{off}}(\ell) J_2(\ell\theta), \quad (13)$$

where $J_2(x)$ is the second-order Bessel function and $\kappa_{M,\text{off}}(\ell)$ is the Fourier transform of the lensing profile taking into account the miscentering effect. In Oguri & Takada (2011), the authors consider a model of $\kappa_{M,\text{off}}$ as follows:

$$\kappa_{M,\text{off}}(\ell) = \kappa_M(\ell) \left[f_{\text{cen}} + (1 - f_{\text{cen}}) \exp \left(-\frac{1}{2} \sigma_s^2 \ell^2 \right) \right], \quad (14)$$

where κ_M is the Fourier transform of Equation (9), f_{cen} is the fraction of central galaxies located at the real center of the halo, and σ_s is the variance of the offset distances between the position of the central galaxies and the halo centers.

In observations, off centering can occur either because the adopted cluster-finding algorithm fails in some way, or because there is a *real* physical offset between the center of the halo and the position of the central galaxy. In the former case, one can estimate the overall effect by using the mock cluster catalog based on, for example, N -body simulations. Johnston et al. (2007) use simulations to compare the centers of halos and the centers of clusters identified by their cluster

finding algorithm. They find that the offset due to the misidentification is well described by a two-dimensional Gaussian form with a variance of $0.42 h^{-1}$ Mpc. Hilbert & White (2010) also perform a similar analysis and find a similar value of variance of $0.34\text{--}0.41 h^{-1}$ Mpc for different cosmological models. Motivated by these results, Oguri & Takada (2011) set $f_{\text{cen}} = 0.75 \ln(M/3 \times 10^{14} h^{-1} M_{\odot})$ and $\sigma_s D_1 = 0.42 h^{-1}$ Mpc as fiducial model parameters in their analysis. We adopt the same parameters as our fiducial model.

At length scales larger than the virial radii of host halos, neighboring halos are the dominant contribution to the lensing observable. With the Limber approximation, the so-called two-halo contribution is calculated as (see, e.g., Oguri & Hamana 2011)

$$\gamma_{t,2h}(\theta) = \int \frac{\ell d\ell}{2\pi} \frac{\bar{\rho}_m(z) b_h(M)}{(1+z)^3 \Sigma_{\text{crit}} D_1} P_m(k_\ell, z) J_2(\ell\theta), \quad (15)$$

where $k_\ell = \ell/[D_1(1+z)]$, $P_m(k)$ is the linear matter power spectrum, and $b_h(M)$ is the halo bias. Throughout this paper, we calculate $P_m(k)$ using CAMB (Lewis et al. 2000). We adopt the halo bias model with the virial overdensity of $\Delta = 200$ developed in Tinker et al. (2010). To remain consistent with our calculation in Equation (15), we convert the mass of the host halo using the definition of Δ from Hu & Kravtsov (2003).

Using the above models, we can calculate the lensing observable of central galaxies for a given redshift z and host halo mass M by the sum of Equations (13) and (15).

Satellite Galaxies

The excess surface mass density around satellite galaxies $\Delta\Sigma_{\text{sat}}$ is expressed as

$$\Delta\Sigma_{\text{sat}}(R) = \Delta\Sigma_{\text{sat,sub}}(R) + \Delta\Sigma_{\text{sat,host}}(R|R_{\text{off}}), \quad (16)$$

where $\Delta\Sigma_{\text{sat,sub}}$ is the contribution from the subhalo around satellite galaxies, $\Delta\Sigma_{\text{sat,host}}$ is the excess surface mass density due to the host halo, and R_{off} is the offset between the position of satellite galaxies and the center of the host halo.

For the density profile of a subhalo, we adopt the following functional form proposed by Hayashi et al. (2003),

$$\rho_{\text{sub}}(r) = \frac{\rho_{s,\text{sub}}}{(r/r_{s,\text{sub}})(1+r/r_{s,\text{sub}})^2} \left(\frac{r_{t,\text{sub}}^3}{r^3 + r_{t,\text{sub}}^3} \right). \quad (17)$$

Using high-resolution numerical simulations, Hayashi et al. (2003) shows that the effective tidal radius $r_{t,\text{sub}}$ is expressed by a function of the mass fraction f_m of the subhalo that remains bound:

$$\log \left(\frac{r_{t,\text{sub}}}{r_{s,\text{sub}}} \right) = 1.02 + 1.38 + \log f_m + 0.37 (\log f_m)^2. \quad (18)$$

Gao et al. (2004) calculate the radial dependence of f_m for a large set of subhalos located in a large cosmological N -body simulation. They find the mean relation between the offset from the center of halo and f_m , which is given by

$$f_m = 0.65 \left(\frac{r_{\text{off}}}{r_{\text{vir,host}}} \right)^{2/3}, \quad (19)$$

where r_{off} is the distance of the subhalo from the center of the host halo and $r_{\text{vir,host}}$ is the virial radius of the host halo. We specify the scale density and radius for subhalos through the concentration parameter in the same way as for host halos. For the concentration parameter of subhalos, we adopt the model in Bullock et al. (2001). Bullock et al. (2001) have shown that the subhalos in high-density region tend to be more concentrated than isolated halos. Although this trend is only marginal due to a large scatter, we adopt their result in our analysis. However, this choice does not significantly change the result shown in the forecast section in this paper. We thus calculate $\Delta\Sigma_{\text{sat,sub}}$ by replacing $\bar{\rho}_m \xi_{g,m}$ with ρ_{sub} in Equation (3). In the Appendix, we compare the model of subhalo density profile by Equation (17) with the measured density profiles for the subhalos in our cosmological simulation. There, we find that the overall feature of the subhalo density profile can be well described by Equation (17), at least for the massive subhalos with the mass of $\sim 10^{12} h^{-1} M_\odot$.

The contribution from the density profile of host halos is given by (see, e.g., Yang et al. 2006)

$$\Delta\Sigma_{\text{sat,host}}(R|R_{\text{off}}) = \frac{1}{\pi R^2} \int_0^R 2\pi R' \int_0^{2\pi} \Sigma_{\text{host}}(R'_\theta) d\theta dR' - \frac{1}{2\pi} \int_0^{2\pi} \Sigma_{\text{host}}(R_\theta) d\theta, \quad (20)$$

where $R_\theta = \sqrt{R^2 + R_{\text{off}}^2 + 2R_{\text{off}}R \cos \theta}$ and $\Sigma_{\text{host}}(R)$ is the surface mass density of the host halo given by multiplying Σ_{crit} and $\kappa_h(R)$ in Equation (9).

One may think that, in order to probe the subhalo density profile with galaxy–galaxy lensing analysis, a priori knowledge of the offset length R_{off} for each satellite galaxy is necessary. In the following section, we propose a novel method to select satellite galaxies in galaxy groups and clusters *without* identifying the center of the host halos.

2.2. Selection Method

Our selection method is based on the lensing mass map reconstructed from the observed shear of each background galaxy. We first define the lensing mass map, i.e., the smoothed lensing convergence field:

$$\mathcal{K}(\boldsymbol{\theta}) = \int d^2\phi \kappa(\boldsymbol{\theta} - \boldsymbol{\phi}) U(\boldsymbol{\phi}), \quad (21)$$

where U is the filter function specified below. We can calculate the same quantity by smoothing the shear field γ as

$$\mathcal{K}(\boldsymbol{\theta}) = \int d^2\phi \gamma_t(\boldsymbol{\phi} : \boldsymbol{\theta}) Q_t(\boldsymbol{\phi}), \quad (22)$$

where γ_t is the tangential component of the shear at position ϕ relative to the point θ . The filter function for the shear field Q_t is related to U by

$$Q_t(\theta) = \int_0^\theta d\theta' \theta' U(\theta') - U(\theta). \quad (23)$$

We consider Q_t to have a finite extent. In this case, one finds

$$U(\theta) = 2 \int_\theta^{\theta_o} d\theta' \frac{Q_t(\theta')}{\theta'} - Q_t(\theta), \quad (24)$$

where θ_o denotes the outer boundary of the filter function.

Various functional forms of Q_t have been proposed for identifying galaxy clusters (e.g., Hamana et al. 2004; Hennawi & Spergel 2005; Maturi et al. 2005; Hamana et al. 2012). In the following, we use a truncated Gaussian filter (for U) as

$$U(\theta) = \frac{1}{\pi\theta_{\text{sm}}^2} \exp\left(-\frac{\theta^2}{\theta_{\text{sm}}^2}\right) - \frac{1}{\pi\theta_o^2} \left(1 - \exp\left(-\frac{\theta_o^2}{\theta_{\text{sm}}^2}\right)\right), \quad (25)$$

$$Q_t(\theta) = \frac{1}{\pi\theta^2} \left[1 - \left(1 + \frac{\theta^2}{\theta_{\text{sm}}^2}\right) \exp\left(-\frac{\theta^2}{\theta_{\text{sm}}^2}\right)\right], \quad (26)$$

for $\theta \leq \theta_o$ and $U = Q_t = 0$ elsewhere. In this case, $\theta Q_t(\theta)$ has a maximum at the angular scale of $\sim 2\theta_{\text{sm}}$.

The first step of our selection method is to calculate the lensing mass \mathcal{K} at the position of each galaxy in a group of galaxies. The average profile of the tangential shear around satellite galaxies would be negative at the offset length (Yang et al. 2006). We then expect that the resulting \mathcal{K} at the position of the satellite galaxies show, *statistically*, negative values if the offset length is similar to the scale of smoothing (corresponding to $2\theta_{\text{sm}}$ in our case). Figure 1 illustrates the essence of our selection method. The solid lines show the expected lensing signal γ_t due to the satellite galaxies with the different offset length, for the halo mass $M_{\text{host}} = 10^{14} h^{-1} M_\odot$ and the subhalo mass $M_{\text{sub}} = 10^{11.5} h^{-1} M_\odot$ at $z = 0.15$ and the source redshift $z_{\text{source}} = 1$. The dashed line in Figure 1 indicates our filter $\theta Q_t(\theta)$ with $\theta_{\text{sm}} = 1$ arcmin and the arbitrary normalization. The model cluster has a virial radius of $\theta_{\text{vir}} \sim 8$ arcmin. By setting the smoothing scale to be 1 arcmin, one can select the satellite galaxies with the offset length of $\sim 2\theta_{\text{sm}}/\theta_{\text{vir}}$ by searching for the negative \mathcal{K} at the position of each member galaxy in the group.

Let us consider a simple configuration of a host halo and a subhalo as shown in Figure 2. The top left panel represents the lensing signals κ and γ assuming the halo mass $M_{\text{host}} = 10^{14} h^{-1} M_\odot$ and subhalo mass $M_{\text{sub}} = 10^{11.5} h^{-1} M_\odot$ at $z = 0.15$ and the source redshift $z_{\text{source}} = 1$. The subhalo is offset from the center of the host halo with length of $0.3\theta_{\text{vir}}$. We show the positive and negative tangential shear pattern with respect to the position of the subhalo in the bottom left panel. The positive and negative shear are expressed by red and blue lines, respectively. Clearly, the negative shear pattern appears around the subhalo. The bottom right panel shows the integrand

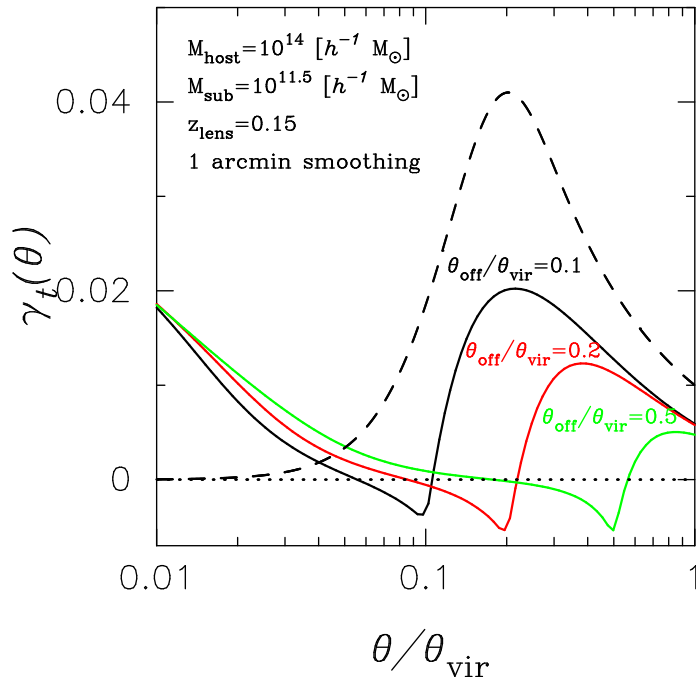


Fig. 1.— Expected lensing signal around subhalos for the source redshift $z_{\text{source}} = 1$. Three lines show the lensing signal for the satellite galaxies with different offset lengths. The black, red, and green lines correspond to $\theta_{\text{off}}/\theta_{\text{vir}} = 0.1, 0.2,$ and 0.5 , respectively. In this figure, we assume a host halo with mass $M_{\text{host}} = 10^{14} h^{-1} M_{\odot}$ at $z = 0.15$ and a subhalo mass $M_{\text{sub}} = 10^{11.5} h^{-1} M_{\odot}$. The dashed line shows the window function for the selection process with a smoothing scale of 1 arcmin. The normalization of the window function is arbitrary.

of Equation (22) ($Q_t \gamma_t$) around the subhalo. In this panel, we adopt Gaussian smoothing with $\theta_{\text{sm}} = 0.5$ arcmin. The summation over the pixel in the bottom right panel yields the smoothed convergence \mathcal{K} at the position of the subhalo. The main contribution in Equation (22) comes from $\theta = 2\theta_{\text{sm}}$ shown by the blue dashed line in the bottom right panel. These panels indicate that the resulting \mathcal{K} at the position of the subhalo would be negative even in a high density region when a subhalo is offset from the center of the host halo.

We emphasize that our method does not extract the information of the density profiles of subhalos. Our selection instead relies on the shear signal contributed by the host halo. The point of our selection is to consider the shear signal of the host halo at *the position of the subhalos*. The measured shear around the subhalos would be negative in principle when the angular separation is equal to the projected distance between the subhalo and host halo center. This means that we can measure the offset distance of the subhalos by searching for the negative contribution of the measured shear at the position of the subhalos. In our selection method we try to extract the negative value of the shear profile around the subhalos by using the filter $Q(\theta)$ with a smoothing

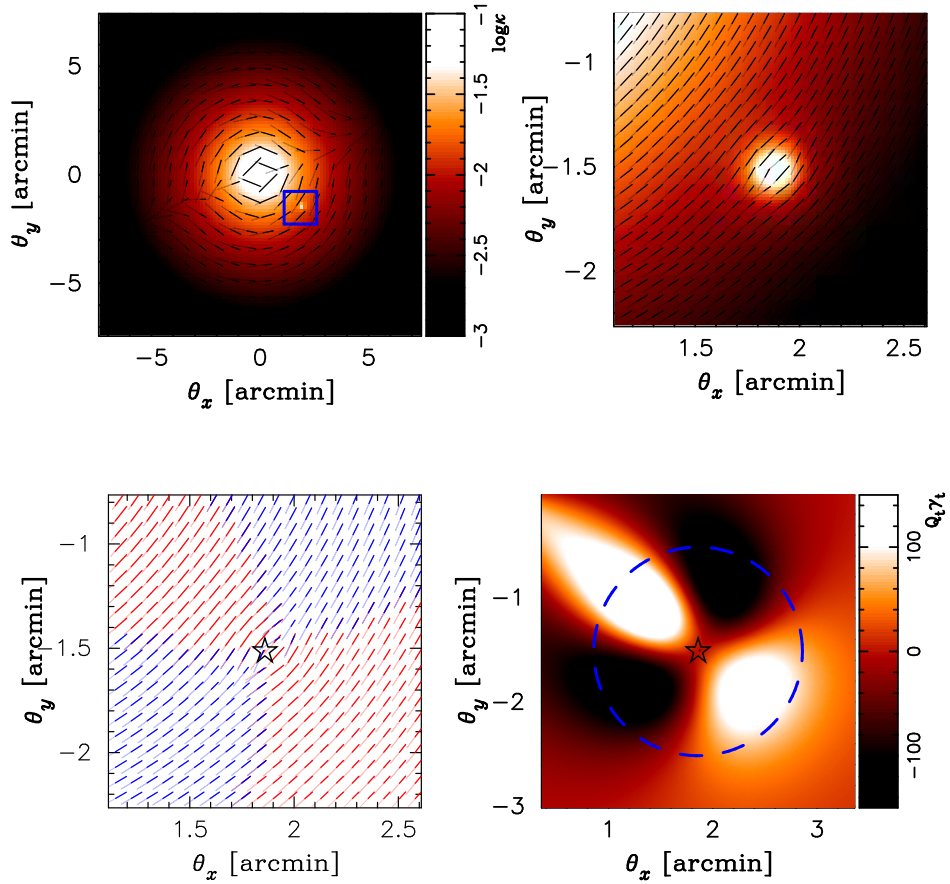


Fig. 2.— Simple example of our selection method. The top left panel shows the expected lensing signal due to a host halo and subhalo for the source redshift $z_{\text{source}} = 1$. In the top left panel, the color coordinate represents convergence and the black line shows shear. In all panels of this figure we assume a host halo with mass $M_{\text{host}} = 10^{14} h^{-1} M_{\odot}$ at $z = 0.15$ and subhalo mass $M_{\text{sub}} = 10^{11.5} h^{-1} M_{\odot}$. The offset length is set to be $0.3\theta_{\text{vir}}$ with $\theta_{\text{vir}} = 8$ arcmin. The top right panel is a zoom-in image around the subhalo. The bottom left panel shows the positive and negative tangential shear at the position of the subhalo. The positive (negative) shear is expressed by red (blue) lines. The bottom right panel shows the integrand in Equation (22). The normalization of the window function is arbitrary. The dashed line in the bottom right panel corresponds to the circle with a radii of $\theta = 2\theta_{\text{sm}}$, which is the main contribution in the integral of Equation (22). We adopt Gaussian smoothing with $\theta_{\text{sm}} = 0.5$ arcmin.

scale adjusted by the offset distance of interest.

The reconstruction of the lensing mass map is effected by a number of systematics, such as the intrinsic noise, the projection effect of the large-scale structure, and the diversity of dark matter distribution in clusters. We thus examine our method by using numerical simulations and taking

account of these effects in Section 3. Throughout this paper, we adopt $\theta_{\text{sm}} = 1$ arcmin and $\theta_o = 15$ arcmin. Note that the choice of θ_{sm} is thought to be an optimal smoothing scale for the detection of massive galaxy clusters using weak-lensing for $z_{\text{source}} = 1.0$ (Hamana et al. 2004). The value of θ_{sm} can also be set by the desired offset length of member galaxies in principle. Interestingly, we find that the final result does not change significantly when the smoothing scale is varied in the range of 1–2 arcmin, because our filter function has a large characteristic width. The optimization of the filter function would be important for improving the statistical power of the method. In this paper, we simply show the validity of our proposed method and leave the optimization for future works.

3. TEST OF SELECTION METHOD

3.1. Simulation Data

We first run a number of cosmological N -body simulations to generate a three-dimensional matter density field. We use the parallel Tree-Particle Mesh code `Gadget2` (Springel 2005). The simulations are run with 1024^3 dark matter particles in a volume of $200 h^{-1}\text{Mpc}$ on a side. We generate the initial conditions using a parallel code developed by Nishimichi et al. (2009) and Valageas & Nishimichi (2011), which employs the second-order Lagrangian perturbation theory (e.g., Crocce et al. 2006). The initial redshift is set to $z_{\text{init}} = 49$, where we compute the linear matter transfer function using `CAMB` (Lewis et al. 2000). Our fiducial cosmology adopts the following parameters: matter density $\Omega_{\text{m}0} = 0.272$, dark energy density $\Omega_{\Lambda 0} = 0.728$, the density fluctuation amplitude $\sigma_8 = 0.809$, the parameter of the equation of state of dark energy $w_0 = -1$, Hubble parameter $h = 0.704$ and the scalar spectral index $n_s = 0.963$. These parameters are consistent with the *WMAP* seven-year results (Komatsu et al. 2011).

For ray-tracing simulations of gravitational lensing, we generate light-cone outputs using multiple simulation boxes in the following manner. Our simulations are placed to cover the past light-cone of a hypothetical observer with an angular extent $4^\circ \times 4^\circ$, from $z = 0$ to 1, similar to the methods in White & Hu (2000), Hamana & Mellier (2001), and Sato et al. (2009). Details of the configuration are found in the last reference. The angular grid size of our maps is $4^\circ/4096 \sim 0.06$ arcmin. We randomly shift the simulation boxes in order to avoid the same structure appearing multiple times along a line-of-sight. In total, we generate 50 independent shear maps with the source redshift $z_{\text{source}} = 1$ from our N -body simulation. It is known that the intrinsic ellipticities of source galaxies induce noise to lensing shear maps. We model the noise by adding random ellipticities drawn from the following distribution to the simulated shear data (Hamana et al. 2012):

$$P(|e|) = \frac{1}{\pi\sigma_e^2(1 - e^{-1/\sigma_e^2})} \exp\left(-\frac{e^2}{\sigma_e^2}\right), \quad (27)$$

$$\sigma_e = \frac{\sigma_{\text{int}}}{\sqrt{n_{\text{gal}}\theta_{\text{pix}}^2}}, \quad (28)$$

where σ_{int} is the root-mean-square of intrinsic ellipticities, n_{gal} is the number density of source galaxies, and $\theta_{\text{pix}} = 0.06$ arcmin. We set σ_{int} to be 0.4 and assume $n_{\text{gal}} = 10 \text{ arcmin}^{-2}$. These are typical values for a weak lensing survey using the Canada–France–Hawaii Telescope (Erben et al. 2013).

In each output of the N -body simulation, we locate dark matter halos using the standard friend-of-friend (FOF) algorithm with the linking parameter of $b = 0.2$. We define the mass of each halo by the spherical overdensity mass with $\Delta = 200$, which is denoted by M_{200} . The position of each halo is defined by the position of the particle located at the potential minimum in each FOF group. We then find the self-bound, locally overdense region in each FOF group by SUBFIND (Springel et al. 2001). For the subhalo catalog, the minimum number of particles is set to be 30. This choice corresponds to the minimum subhalo mass, which is $\sim 10^{10} h^{-1} M_{\odot}$. We thus expect that the position of subhalos with a mass of $\sim 10^{10} h^{-1} M_{\odot}$ would be identified in our simulation. However, the resolution seems to be insufficient to investigate the density profile of subhalos with a mass of $\sim 10^{10} - 10^{11} h^{-1} M_{\odot}$. In order to get the largest samples possible for stacking analysis in the following, we use all subhalos with 30 particles or more. In the following analysis, we use halos with a mass greater than $10^{13} h^{-1} M_{\odot}$. Using the FOF halos, we construct mock group catalogs on the light cone by arranging the simulation outputs in the same manner as the ray-tracing simulation. We mark the positions of the halos and their subhalos in the shear map. In summary, our mock catalogs contain data about the masses, redshifts, and angular positions on the shear map for the halos and subhalos. We regard the subhalos in each halo as satellite galaxies. We define the center of each group on the sky as the local highest peak of the convergence map within the virial radius from the halo position. For determination of the center, we only consider the nearest halo for each convergence peak when multiple halos are aligned on a line-of-sight. Thus, the position of a halo does not always correspond to the position of the highest convergence peak. Nevertheless, we have checked that the stacking signal around halos is reproduced as in Oguri & Hamana (2011) with our definition of the center. Unfortunately, we cannot find the lensing signal due to subhalos in our simulations. This is because the final result of stacking signals mainly contains the information of the subhalos with a mass of $10^{10} - 10^{11} h^{-1} M_{\odot}$ on small angular scales. We thus resort to comparing the resulting signals with the theoretical model of the contribution from the host halo, (i.e., $\Delta\Sigma_{\text{sat,host}}(R|R_{\text{off}})$ in Equation (16)) as a test of our method.

3.2. Result

We apply the method described in Section 2.2 to our mock group catalogs. For a given group, we calculate \mathcal{K} at the position of each subhalo using Equation (22). We then select subhalos with the negative \mathcal{K} for stacking analysis. We repeat the selection over 50 shear maps independently. The total sky coverage for stacking analysis in this section reaches $50 \times 4^{\circ} \times 4^{\circ} = 800 \text{ deg}^2$. The average tangential shear profile over the selected subhalos is computed as a function of the angular separation θ . In binning θ , we set $\Delta\theta = 0.1$ arcmin in the range from 0 to 10 arcmin. We perform

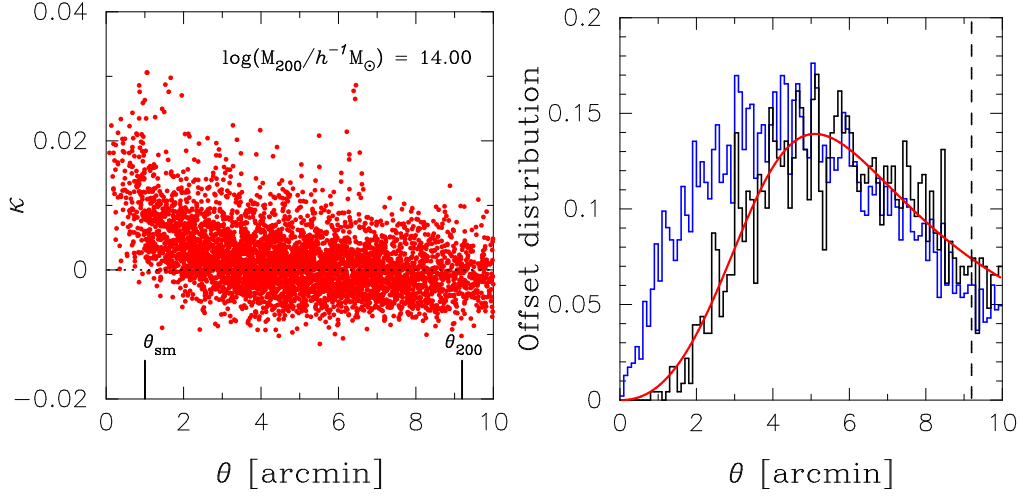


Fig. 3.— Left panel shows the scatter plot of \mathcal{K} as a function of the offset angle. In this figure, we use 5448 subhalos with the host halo mass of $M_{200} = 10^{13.9} - 10^{14.1} h^{-1}M_{\odot}$ and the redshift range of 0.1–0.2. For reference, we show the smoothing scale θ_{sm} and θ_{200} in the left panel. The offset distribution of the selected subhalos by our method is shown in the right panel by the solid line. The dashed line in the right panel corresponds to θ_{200} . The red line in the right panel shows the fitting by the function in Equation (31). The blue histogram represents the offset distribution of all subhalos.

this analysis for the groups at $z = 0.1 - 0.2$. We consider four mass bins centered at $M_{200} = 10^{13.5}$, $10^{13.75}$, $10^{14.0}$, and $10^{14.25} h^{-1}M_{\odot}$ with logarithmic bin size of $\Delta \log(M_{200}) = 0.1$. In the stacking analysis we used 7278, 7046, 5448, and 995 subhalos for each host halo mass bin $M_{200} = 10^{13.5}$, $10^{13.75}$, $10^{14.0}$, and $10^{14.25} h^{-1}M_{\odot}$, respectively.

The left panel in Figure 3 shows the scatter plot of \mathcal{K} as a function of the offset length between the position of the subhalo and the center of the group halo. For this figure, we use groups with masses of $M_{200} = 10^{13.9} - 10^{14.1} h^{-1}M_{\odot}$. As shown in the left panel in Figure 3, our method selects subhalos with a larger offset scale than smoothing scale. It has a high success rate of selection for the subhalos well separated from the center of each main halo, that is most subhalos are off-centered with the distance of $\gtrsim 2\theta_{\text{sm}}$ when they show the negative \mathcal{K} . The efficiency and purity of the selection method is quite important to show how our method works. We define the efficiency and purity as follows,

$$\text{Efficiency} = \frac{\text{the number of subhalos with } \theta_{\text{off}} > \theta_{\text{sm}} \text{ and } \mathcal{K} < 0}{\text{the number of subhalos with } \theta_{\text{off}} > \theta_{\text{sm}}}, \quad (29)$$

$$\text{Purity} = \frac{\text{the number of subhalos with } \theta_{\text{off}} > \theta_{\text{sm}} \text{ and } \mathcal{K} < 0}{\text{the number of subhalos with } \mathcal{K} < 0}, \quad (30)$$

where θ_{off} is the projected distance between the subhalo and the host halo, and $\theta_{\text{sm}} = 1$ arcmin is the smoothing scale of our method. We found that the purity reaches almost 100% and the

efficiency is $\sim 40\%$ for four mass bins. The result is summarized in Table 1. The right panel in Figure 3 shows the offset distribution of the selected subhalos. In the outer region ($\theta/\theta_{\text{vir}} \gtrsim 0.5$), the distribution of the offset lengths of the selected subhalos traces that of all subhalos, but the inner slope of the offset distribution becomes steeper. This is likely caused by our selection; our method is effective only for the subhalos in the outer region and the subhalos near the center of the group are not detected. We find the resulting offset distribution is well described by the following functional form:

$$P(\theta) = A \frac{\theta^{p_1}}{1 + (p_2 \theta)^{p_3}}, \quad (31)$$

where A is a normalization factor given by $\int d\theta P(\theta) = 1$. Using the offset distribution, the expected lensing signals due to the host halos (i.e., $\Delta\Sigma_{\text{sat,host}}(R|R_{\text{off}})$ in Equation (16)) are expressed by

$$\int d\theta_{\text{off}} P(\theta_{\text{off}}) \Delta\Sigma_{\text{sat,host}}(\theta|\theta_{\text{off}}), \quad (32)$$

where $\theta_{\text{off}} = R_{\text{off}}/D_1$ and $\theta = R/D_1$.

It is important to consider an additional effect or bias caused by our subhalo selection. Because we only use the point with the negative \mathcal{K} for galaxy–galaxy lensing analysis, the stacked lensing signals are intrinsically biased. In order to extract the contribution from the host halo, we need to correct the negative bias. Let us separate the observed shear γ_{obs} into the three components:

$$\gamma_{\text{obs}} = \gamma_{\text{obj}} + \gamma_{\text{LSS}} + \gamma_{\text{N}}, \quad (33)$$

where γ_{obj} corresponds to the lensing signal due to the halo or/and subhalo, γ_{LSS} is the contribution from the projection of the large-scale structure and γ_{N} is the contribution from the intrinsic shape noise of the source galaxies. In our selection, we use the lensing mass map \mathcal{K} defined by Equation (22). The field \mathcal{K} is similarly decomposed into the three contributions \mathcal{K}_{obj} , \mathcal{K}_{LSS} , and \mathcal{K}_{N} . Even in the case of no lensing signals (i.e., $\gamma_{\text{obj}} = \gamma_{\text{LSS}} = 0$), there remains a nonvanishing effect after stacking the points where $\mathcal{K} < 0$. We denote this term $\langle \gamma_{\text{N}} \rangle_{\mathcal{K} < 0}$. It can be estimated from the measured shear directly by rotating the orientation of the observed ellipticities randomly and then stacking the random points where $\mathcal{K} < 0$ in the randomized catalogs. There is a similar non-vanishing contribution in the case of $\gamma_{\text{N}} = 0$, which is denoted by $\langle \gamma_{\text{LSS}} \rangle_{\mathcal{K} < 0}$. The contribution can be evaluated by stacking the random points where $\mathcal{K} < 0$ in the lensing shear maps without the intrinsic noise. One can estimate the large-scale structure contribution in principle by assuming that γ_{LSS} follows a specific probability distribution function such as a Gaussian. For our purpose, we simply estimate $\langle \gamma_{\text{LSS}} \rangle_{\mathcal{K} < 0}$ by stacking the random points where $\mathcal{K} < 0$ over 50 simulated shear maps without intrinsic noises. In the presence of both noise and the cosmic signal due to large-scale structure, the expected offset signal would be expressed by the linear combination of $\langle \gamma_{\text{LSS}} \rangle_{\mathcal{K} < 0}$ and $\langle \gamma_{\text{N}} \rangle_{\mathcal{K} < 0}$. We find that the lensing profile due to host halos can be reproduced by subtracting the contribution (bias) in the following form from the observed lensing signals around the points where $\mathcal{K} < 0$:

$$f_{\text{LSS}} \langle \gamma_{\text{LSS}} \rangle_{\mathcal{K} < 0} + \langle \gamma_{\text{N}} \rangle_{\mathcal{K} < 0}, \quad (34)$$

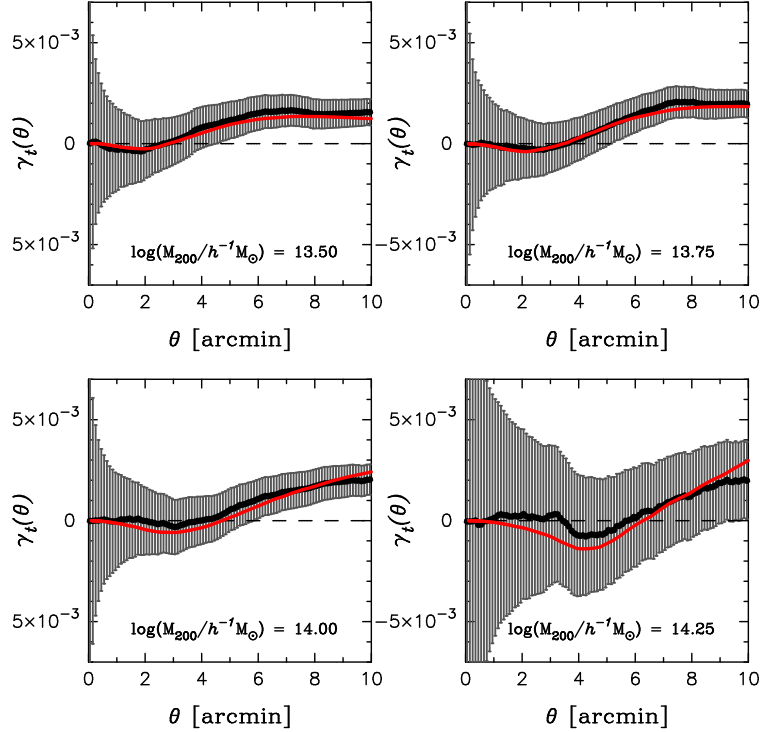


Fig. 4.— We compare the measured lensing signal with our theoretical model. The black points show the measured lensing signal averaged over 50 mock shear maps (800 deg^2) and group catalogs. The correction for the nonzero random signal is performed. The red lines show our theoretical model with the offset distribution fitted by the function in Equation (31). The gray error bars in each panel show the statistical error of galaxy–galaxy lensing analysis for 800 deg^2 assuming $\sigma_{\text{int}} = 0.4$ and $n_{\text{gal}} = 10 \text{ arcmin}^{-2}$.

where f_{LSS} is the fraction of the points where $\mathcal{K}_{\text{LSS}} < 0$ among the points where $\mathcal{K}_{\text{LSS}} + \mathcal{K}_{\text{N}} < 0$. Using the mock catalog and the ray-tracing simulation, we can directly measure this fraction f_{LSS} over all selected points where $\mathcal{K} < 0$. We find that the typical value of f_{LSS} is ~ 0.7 in the mass range of $10^{13.5-14.25} h^{-1} M_\odot$. We summarize the parameter related to our selection p_1, p_2, p_3 and f_{LSS} in Table 1.

Figure 4 shows the comparison with the measured lensing signal by our selection method and the theoretical model described by Equation (32). The black points show the measured lensing signals around the subhalos with the negative \mathcal{K} after subtracting the contribution shown in Equation (34). To correct the selection bias, we use the measured value of f_{LSS} from 50 shear maps directly. The red lines show the theoretical models with the resulting offset distribution. For the calculation of the model, we fit the resulting offset distribution from our selection method by the function in Equation (31). The gray error bars represent the statistical error of our stacking anal-

	N_{sub}	$N_{\text{sub,selec}}$	Efficiency	Purity	p_1	p_2 [arcmin ⁻¹]	p_3	f_{LSS}
$M_{200} = 10^{13.5} h^{-1} M_{\odot}$	7278	3049	3016/6920	3016/3049	1.64	0.253	4.40	0.669
$M_{200} = 10^{13.75} h^{-1} M_{\odot}$	7046	2840	2827/6747	2827/2840	1.70	0.217	4.56	0.715
$M_{200} = 10^{14} h^{-1} M_{\odot}$	5448	2289	2287/5294	2287/2289	2.27	0.200	4.31	0.744
$M_{200} = 10^{14.25} h^{-1} M_{\odot}$	995	353	353/965	353/353	8.53	0.248	9.38	0.793

Table 1: The parameters in galaxy–galaxy lensing analysis with our selection method. We use the host halos with the redshift of 0.1 – 0.2. N_{sub} is the total number of subhalos used in the analysis and $N_{\text{sub,selec}}$ is the number of selected subhalos. p_1 , p_2 , and p_3 are parameters for the resulting offset distribution, and f_{LSS} represents the correction factor for the mean signal around random points. Details are found in the text.

ysis over 50 realizations of shear maps, assuming $\sigma_{\text{int}} = 0.4$ and $n_{\text{gal}} = 10 \text{ arcmin}^{-2}$. After the correction as shown in Equation (34), and using the offset distribution given by Equation (31), we can successfully reproduce the lensing signal originated from the contribution of the host halo at the off-centered position.

4. FORECAST

We present a forecast for constraining the statistical properties of subhalos (satellites) in galaxy groups with the method developed in Section 3 for upcoming lensing surveys. We consider two wide surveys with an area coverage of 1400 deg² and 20,000 deg²; the former corresponding to Subaru Hyper Suprime-Cam (HSC), and the latter to Large Synoptic Survey Telescope (LSST).

We perform a Fisher analysis to forecast the constraints on the mean subhalo density profile. For a multivariate Gaussian likelihood, the Fisher matrix F_{ij} is written as

$$F_{ij} = \frac{1}{2} \text{Tr} [A_i A_j + C^{-1} M_{ij}], \quad (35)$$

where $A_i = C^{-1} \partial C / \partial p_i$, $M_{ij} = 2 (\partial \gamma_t(\mathbf{p}) / \partial p_i) (\partial \gamma_t(\mathbf{p}) / \partial p_j)$, C is the data covariance matrix and $\gamma_t(\mathbf{p})$ is the theoretical prediction of the lensing observable for central galaxies or for satellite galaxies as a function of parameters of interest². In the present study, we choose 11 parameters to constrain as follows:

$$\mathbf{p} = (M_{200}, c_{\text{vir}}, f_{\text{cen}}, \sigma_s, p_1, p_2, p_3, f_{\text{LSS}}, M_{\text{sub}}, c_{\text{sub}}, \tau_{\text{sub}}), \quad (36)$$

where M_{200} is the mean mass of host halos, c_{vir} is the concentration parameter of host halos, f_{cen} and σ_s are associated with the off-centering effect of central galaxies in the group, M_{sub} is the mean mass

² We only consider the second term in Equation (35). Because C scales approximately inversely proportionate to the survey area, the second term is expected to be dominant for a very wide area survey.

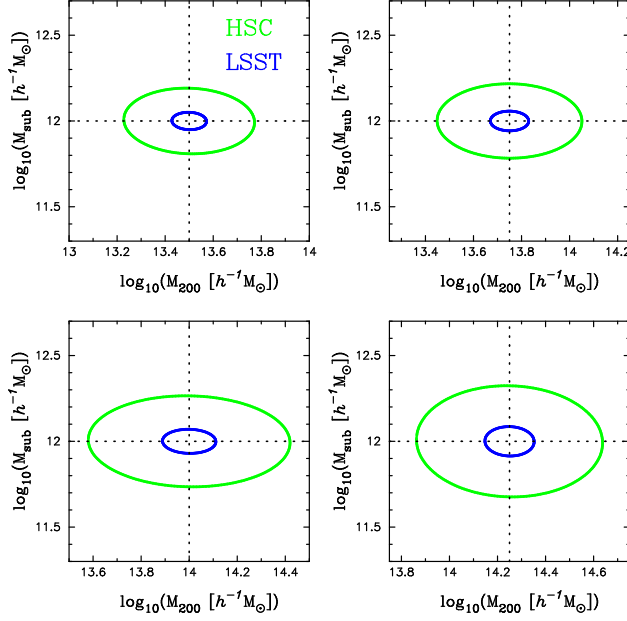


Fig. 5.— We plot 1σ confidence level in $M_{\text{sub}} - M_{200}$ plane by galaxy–galaxy lensing analysis with the selection method proposed in this paper. The green circle in each panel represents the constraints for Subaru HSC survey (1400 deg^2), whereas the blue circle is for LSST survey ($20,000 \text{ deg}^2$).

of selected subhalos, c_{sub} is the concentration parameter of selected subhalos, $\tau_{\text{sub}} = r_{t,\text{sub}}/r_{s,\text{sub}}$ is the dimensionless tidal radius of subhalos, and p_1 , p_2 , p_3 and f_{LSS} are parameters related to our selection method. For the Fisher analysis, we consider the four mass bins of $M_{200} = 10^{13.50 \pm 0.1}$, $10^{13.75 \pm 0.1}$, $10^{14.00 \pm 0.1}$, and $10^{14.25 \pm 0.1} h^{-1} M_{\odot}$ at $z = 0.15 \pm 0.05$. In each mass bin M_{200} , we assume $M_{\text{sub}} = 10^{12} h^{-1} M_{\odot}$ and set the fiducial value of c_{vir} , f_{cen} , σ_s , and c_{sub} as described in Section 2.1. We adopt the fiducial values for the offset distribution parameters (p_1 , p_2 , and p_3) and f_{LSS} as measured by a galaxy–galaxy lensing analysis of mock 50 shear maps in Section 3. From the measured p_1 , p_2 , and p_3 , we calculate the mean offset distance of the subhalos and then estimate τ_{sub} by Equations (18) and (19). Using these 11 parameters, we calculate the lensing signal for the central galaxies and satellite galaxies, over the range of 0–10 arcmin with the bin size of $\Delta\theta = 0.1$ arcmin.

We estimate the covariance matrix of galaxy–galaxy lensing analysis by the following equation:

$$C_{ij} = \frac{\sigma_{\text{int}}^2}{2} \frac{1}{2\pi\theta_i\Delta\theta n_{\text{gal}}N_{\text{stack}}} \delta_{ij}, \quad (37)$$

where $\sigma_{\text{int}} = 0.4$ is the intrinsic shape noise, $n_{\text{gal}} = 10 \text{ arcmin}^{-2}$ is the number density of source galaxies, θ_i is the i th bin of angular separation in a galaxy–galaxy lensing analysis, and N_{stack} represents the number of stacking objects. We then estimate the number of stacking objects N_{stack}

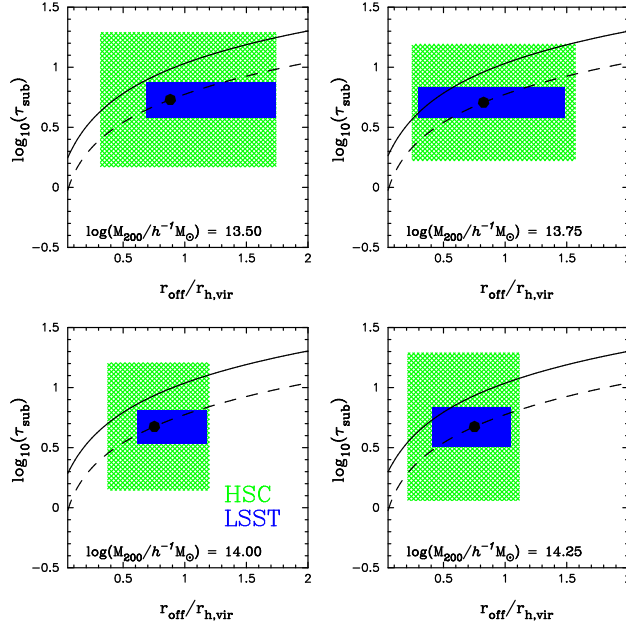


Fig. 6.— We plot 1σ confidence level of τ_{sub} as a function of the mean offset length of selected subhalos. The green patch in each panel represents the constraints for Subaru HSC survey (1400 deg^2), whereas the blue filled region is for LSST survey (20,000 deg^2). The dashed line corresponds to the fiducial model in Equations (18) and (19). The solid line shows another model of the tidal stripping shown in Tormen et al. (1998).

for satellite galaxies by

$$N_{\text{stack}} = f_{\text{selec}} \Omega_{\text{survey}} \int dz \frac{d\chi}{dz} \chi^2 \int dM_{200} \frac{dn_{\text{halo}}}{dM_{200}}(M_{200}, z) N_{200}(M_{200}), \quad (38)$$

where χ is the comoving distance, Ω_{survey} is the area of assumed lensing surveys (1400 or 20,000 deg^2), $dn_{\text{halo}}/dM_{200}$ is the halo mass function in Tinker et al. (2008), and N_{200} is the mass–richness relation. We adopt the mass–richness relation of BCGs shown in Reyes et al. (2008), which is given by $N_{200} = 20 (M_{200}/1.42 \times 10^{14} h^{-1} M_{\odot})^{1/1.16}$. The fraction of selected subhalos by our selection method is denoted by f_{selec} , which is directly estimated from the stacking analysis using the mock shear maps shown in Section 3. f_{selec} is found to be 3049/7278, 2840/7046, 2289/5448, and 353/995 for $M_{200} = 10^{13.50}$, $10^{13.75}$, $10^{14.00}$, and $10^{14.25} h^{-1} M_{\odot}$, respectively. In our simulations, we assume that all the position of subhalos are known. In practice, it is difficult to select member galaxies in the same way as in simulations due to the observational effect (e.g., the magnitude limit of the observation). In this paper, we take into account the selection effect of member galaxies by using the measured mass–richness relation of BCGs in Reyes et al. (2008). Although the fraction of the selected subhalos by our selection method f_{selec} can be dependent on the magnitude limit, f_{selec} does not change significantly if the simulated number density profile of the subhalos is close to that of the observed member galaxies in the outer region of galaxy clusters. We will explore the

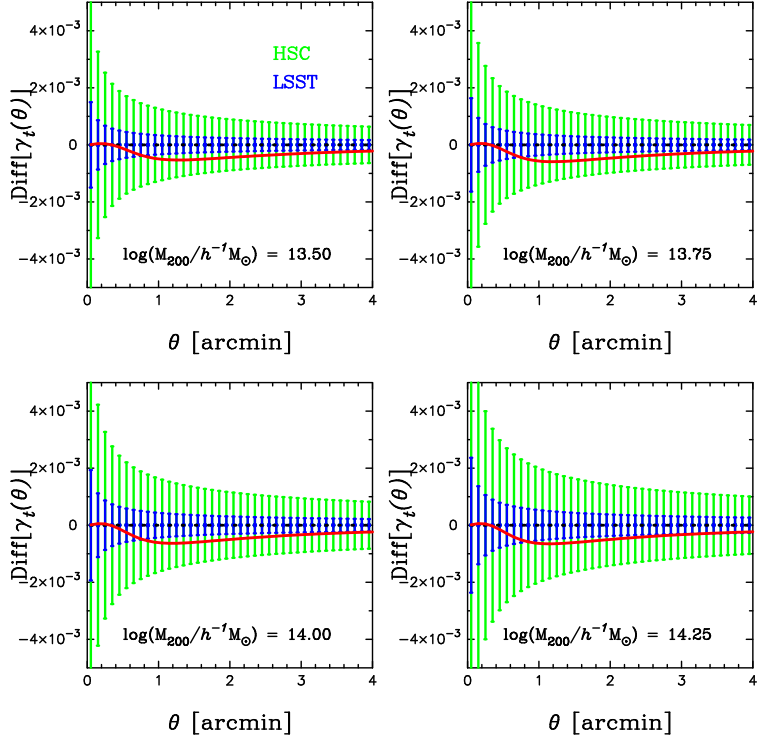


Fig. 7.— Difference between the model of the subhalo profile with and without the cut off in the outer region. The green error bars in each panel represent the statistical error for Subaru HSC survey (1400 deg²), whereas the blue bars are for the LSST survey (20,000 deg²).

selection effect of member galaxies on f_{selec} in future work. In the galaxy–galaxy lensing analysis for central galaxies, N_{stack} is obtained by Equation (38) with $f_{\text{selec}} = 1$ and $N_{200} = 1$. In total, we can calculate the total Fisher matrix by the sum of the contribution from central galaxies and satellite galaxies:

$$\mathbf{F}_{\text{total}}(\mathbf{p}) = \mathbf{F}_{\text{cen}}(M_{200}, c_{\text{vir}}, f_{\text{cen}}, \sigma_s) + \mathbf{F}_{\text{sat}}(M_{200}, c_{\text{vir}}, p_1, p_2, p_3, f_{\text{LSS}}, M_{\text{sub}}, c_{\text{sub}}, \tau_{\text{sub}}). \quad (39)$$

We do not consider the cross-covariance of the lensing signal between central galaxies and satellite galaxies. We expect that the cross covariance would not affect the following results significantly because the lensing signal due to satellite galaxies has weak dependence on the properties of the host halo (i.e., M_{200} and c_{vir}).

We are now able to present a forecast for future lensing surveys covering large sky areas. Figure 5 shows the derived parameter constraints on the mean mass of the halo and subhalo. The green error circles show the 1σ constraints for HSC and the blue circles correspond to the case of LSST. Combined with the stacking signal around central galaxies and the selected satellite galaxies by our method, in the case of HSC, we can constrain the mass of the host halo with a level of $\Delta \log M_{200} = 0.18, 0.20, 0.28,$ and 0.25 for the mass $\log(M_{200}/h^{-1}M_{\odot}) = 13.50, 13.75, 14.00,$ and

14.25 , respectively. Simultaneously, the constraint on the mean mass of the subhalo would reach the level of $\Delta \log M_{\text{sub}} \simeq 0.2$. These constraints can be improved by a factor of ~ 5 for LSST. Figure 6 shows the constraints on the outskirts of the subhalo density profile as a function of the offset scale. The green region in each panel shows the 1σ constraints on the tidal radius of the subhalo τ_{sub} and the mean offset length. The error of the mean offset length is derived from the 1σ error surface in the (p_1, p_2, p_3) space. The dashed line in Figure 6 is the fiducial model of the tidal radius by Equations (18) and (19). For reference, the solid line represents another model of $r_{t,\text{sub}}$ shown in Tormen et al. (1998), which is given by

$$\frac{m_{\text{sub}}(r_{t,\text{sub}})}{r_{t,\text{sub}}^3} = \left(2 - \frac{\partial \ln M_{\text{host}}}{\partial \ln R} \Big|_{R=r_{\text{off}}} \right) \frac{M_{\text{host}}(r_{\text{off}})}{r_{\text{off}}^3}, \quad (40)$$

where $m_{\text{sub}}(r)$ and $M_{\text{host}}(r)$ are the enclosed mass of the subhalo and the halo within r and r_{off} is the separation between the center of the host halo and the position of the subhalo. In Equation (40), we assume the density profile of the host halo and the subhalo as shown in Section 2.1. LSST will enable us to *measure* the tidal radius. We can then observationally verify the model prediction of tidal stripping. Let us consider the differences between the subhalo profile with our fiducial parameter and a model without the cutoff in the outer region (i.e., NFW profile). We denote this difference as $\text{Diff}[\gamma_t(\theta)]$. Figure 7 shows $\text{Diff}[\gamma_t(\theta)]$ for our fiducial parameters. The green error bar in each panel is the statistical error for HSC estimated by Equation (37) and the blue one corresponds to the case of LSST. This figure clearly shows the possibility of distinguishing the tidally stripped profile shown in the Appendix and the simpler NFW profile **with LSST**.

We then explore the lower mass limit of a subhalo by our method. We consider two more cases of subhalo mass: $M_{\text{sub}} = 10^{10} h^{-1} M_{\odot}$ and $M_{\text{sub}} = 10^{11} h^{-1} M_{\odot}$. The fractional error of the subhalo parameters is summarized in Table 2. We find that it is very difficult to put meaningful constraints on the case of a subhalo mass of $10^{10} h^{-1} M_{\odot}$ for any group. Therefore, we conclude that the lower mass limit of the method is $M_{\text{sub}} \sim 10^{11} h^{-1} M_{\odot}$.

We next study the capability of measuring the subhalo density profile with the method proposed in this paper. An important quantity is the cumulative signal-to-noise ratio S/N , which is defined by

$$(S/N)^2 = \sum_{i,j} \gamma_{\text{sat},t}(\theta_i)(\mathbf{p}) C_{ij}^{-1} \gamma_{\text{sat},t}(\theta_j)(\mathbf{p}), \quad (41)$$

where $\gamma_{\text{sat},t}$ is the theoretical prediction of the lensing observable around the selected satellite galaxies by our method. In order to calculate S/N , we consider the fiducial parameters as shown in the previous section, except for M_{sub} and τ_{sub} . For HSC, we can detect the subhalo contribution only for the higher mass and larger tidal radius ($M_{\text{sub}} \gtrsim 10^{12} h^{-1} M_{\odot}$ and $\tau_{\text{sub}} \gtrsim 0.3$) with a level of $\sim 4\sigma$. However, the situation would completely change with LSST. We can detect the subhalo signals with $> 20\sigma$ confidence level over the mass range of $10^{11} - 10^{13} h^{-1} M_{\odot}$, and even in the extreme case of $\tau_{\text{sub}} = 0.1$. This suggests that our method is promising to probe the outskirts of the subhalo density profile and observationally detecting the tidal stripping effect in high density region.

$M_{\text{sub}} = 10^{10} h^{-1} M_{\odot}$	$\sigma(\log(M_{\text{sub}}))/\log(M_{\text{sub}})$	$\sigma(\log(c_{\text{sub}}))/\log(c_{\text{sub}})$	$\sigma(\log(\tau_{\text{sub}}))/\log(\tau_{\text{sub}})$
$M_{200} = 10^{13.5} h^{-1} M_{\odot}$	14.5/10	17.6/1.36	34.4/0.72
$M_{200} = 10^{13.75} h^{-1} M_{\odot}$	22.3/10	27.2/1.36	51.5/0.70
$M_{200} = 10^{14} h^{-1} M_{\odot}$	26.9/10	31.0/1.36	59.4/0.67
$M_{200} = 10^{14.25} h^{-1} M_{\odot}$	39.5/10	46.5/1.36	87.5/0.67
$M_{\text{sub}} = 10^{11} h^{-1} M_{\odot}$	$\sigma(\log(M_{\text{sub}}))/\log(M_{\text{sub}})$	$\sigma(\log(c_{\text{sub}}))/\log(c_{\text{sub}})$	$\sigma(\log(\tau_{\text{sub}}))/\log(\tau_{\text{sub}})$
$M_{200} = 10^{13.5} h^{-1} M_{\odot}$	0.183/11	0.129/1.22	0.503/0.72
$M_{200} = 10^{13.75} h^{-1} M_{\odot}$	0.216/11	0.152/1.22	0.551/0.70
$M_{200} = 10^{14} h^{-1} M_{\odot}$	0.258/11	0.174/1.22	0.620/0.67
$M_{200} = 10^{14.25} h^{-1} M_{\odot}$	0.329/11	0.225/1.22	0.784/0.67
$M_{\text{sub}} = 10^{12} h^{-1} M_{\odot}$	$\sigma(\log(M_{\text{sub}}))/\log(M_{\text{sub}})$	$\sigma(\log(c_{\text{sub}}))/\log(c_{\text{sub}})$	$\sigma(\log(\tau_{\text{sub}}))/\log(\tau_{\text{sub}})$
$M_{200} = 10^{13.5} h^{-1} M_{\odot}$	0.0335/12	0.0228/1.10	0.147/0.72
$M_{200} = 10^{13.75} h^{-1} M_{\odot}$	0.0380/12	0.0225/1.10	0.128/0.70
$M_{200} = 10^{14} h^{-1} M_{\odot}$	0.0464/12	0.0305/1.10	0.140/0.67
$M_{200} = 10^{14.25} h^{-1} M_{\odot}$	0.0567/12	0.0374/1.10	0.162/0.67

Table 2: The forecast of constraints on the properties of subhalo with our selection method. We assume the upcoming survey with a sky coverage of 20,000 deg². We consider the four mass bins of host halos and the three mass bins of subhalos. In every case, the redshift of sources and foreground objects is set to be 1.0 and 0.15, respectively.

5. CONCLUSION AND DISCUSSION

We propose a new method for selecting satellite galaxies in galaxy groups and clusters based on the smoothed lensing mass maps. While we define the center of each group as the maxima of surface mass density, we do not use the information on the relative position of the center throughout our analysis. Our selection scheme is based on the theoretical expectation that the tangential shear around satellite galaxies would show negative value at the offset scale from the center of the host halo. Hence the reconstructed smoothed lensing mass is expected to have a negative value at the off-centered position, even in high density regions such as galaxy clusters, when the smoothing scale is adjusted appropriately. Therefore, one can select the satellite galaxies away from the center of main host halo by measuring the smoothed lensing mass at the position of each galaxy.

We first use high-resolution gravitational lensing simulations to test our selection method in a realistic configuration. We find that the misidentification of the satellite galaxies rarely happens in our selection method even in the presence of intrinsic shape noises, although we cannot select *all* satellite galaxies at a given off-centered position by our method. The measured cosmic shear signal around the selected points in the mock lensing maps can be well described by the sum of the contribution of the host halos, noise due to the large scale structure, and the intrinsic ellipticities. We can model the contribution of the host halos and of the noise to measured lensing signals by

adding four physical parameters associated with the offset distribution of selected members and the calibration for the stacking analysis around biased points.

We then performed a Fisher analysis to demonstrate the constraining power of the density profile around the satellites in the outer region of groups selected by our proposed method. In the case of Subaru Hyper-Suprime Cam (HSC) survey with a sky coverage of 1400 deg^2 , for the galaxy groups at $z = 0.15 \pm 0.05$ with the mass of $M_{200} = 10^{14} h^{-1} M_{\odot}$, we can simultaneously constrain on the subhalo mass and host halo mass with a level of $\sim 0.2 \text{ dex}$ and $\sim 0.3 \text{ dex}$, respectively. These constraints would be improved by a factor of ~ 5 in the case of the Large Synoptic Survey Telescope (LSST) with a wider sky converge of $20,000 \text{ deg}^2$ (see also Table 1). We also consider the detectability of the feature of tidal stripping effects in the stacked shear signals. While we can probe the tidal stripped density profile only for massive subhalos in the case of HSC, we can detect the tidal striping feature for the wide range of subhalo mass of $10^{11} - 10^{13} h^{-1} M_{\odot}$ with a significance level higher than 20σ in the case of LSST.

Our selection method is complementary to another method based on Li et al. (2014) which is based on group catalogs. Here, we consider the comparison with our method and that shown in Li et al. (2014).

The latter always needs the determination of the center of each group. Often, the brightest galaxy in each group is assumed to reside at the center. However, the assumption itself is the potential uncertainty in this methodology. Some simulation studies (e.g., Johnston et al. 2007; Hilbert & White 2010) indicate that the brightest galaxy does not always reside in the center of the host halos. It has been shown that the miscentering of the brightest galaxy could be described by a two-dimensional Gaussian form with a variance of $0.42 h^{-1} \text{ Mpc}$. For groups at $z = 0.15$, this miscentering effect would correspond to the uncertainty of the center with a level of $\sim 3 - 4 \text{ arcmin}$. Under the assumption that the central (brightest) galaxies are at the center, one can easily measure the average cosmic shear signals around the satellites selected by choosing an offset length. Note that the method in Li et al. (2014) uses no additional free parameters in order to extract the contribution of the cosmic shear signals due to subhalos.

On the other hand, our method does not need to use the proxy of the center of each group, because the selection is based on the smoothed lensing mass at the position of member galaxies. Since we measure the stacked shear signals around the biased points in our method, we need the additional free parameters to obtain the cosmic shear signals of interest. Nevertheless, mock weak-lensing catalogs that directly incorporate the actual observational characteristics (e.g., Shirasaki & Yoshida 2014) would be helpful to evaluate the additional parameters and determine their prior probability distribution function. We also need to assume the functional form of the offset distribution of selected members and it seems difficult to select the satellites with a narrow range of the offset length by our proposed method. The optimization of a filter function for smoothed lensing mass might partly mitigate this problem. The simplest way to optimize is to modify the filter so that one can extract the shear signals shown in Figure 1 from observed ellipticities of source galaxies.

The matched filtering scheme (e.g., Hennawi & Spergel 2005) is one of the most useful techniques for extracting the signal of interest. We continue studying the selection method of satellites along this idea.

The reconstructed mass map \mathcal{K} can be also used to determine the center of a group. One simplest way is to find the peak in the \mathcal{K} map around the group of interest. However, in practice, the peak position does not necessarily agree with the center of a group for various reasons (e.g., the presence of substructure in the group, the merger process of the group, and the intrinsic shape noise on \mathcal{K} map). Du & Fan (2014) studied the effect of center offset in \mathcal{K} map with numerical simulations. They found that the variance of the offset between the peak and the true center can be large (\sim the virial radius in the case of $n_{\text{gal}} = 10 \text{ arcmin}^{-2}$). The determination of the center from the \mathcal{K} map is still developing, but can be accurate when the number density of the source galaxies is large or the foreground cluster is very massive. Thus, we expect that our method is useful for wide imaging surveys with a lower number density of source galaxies in order to study the statistical properties of member galaxies. On the other hand, the determination of the center from \mathcal{K} is optimal for deep or targeted imaging surveys with a higher number density of source galaxies for the purpose of understanding the property of individual clusters.

Our proposed method enables us to perform a fundamental test of hierarchical structure formation by revealing whether the tidal stripping (e.g., Hayashi et al. 2003; Gao et al. 2004) occurs efficiently in the outer region of galaxy clusters. Such a test would also be helpful to place constraints on the physical properties of the satellite galaxies in high density regions such as galaxy clusters. One interesting application would be to study the environmental effects on the relation between the subhalo mass and the galaxy properties such as the stellar mass (e.g., Mandelbaum et al. 2006b; Leauthaud et al. 2012), kinematics (e.g., Seljak 2002; Dutton et al. 2010; Reyes et al. 2012), and dust reddening (e.g., Ménard et al. 2010). The resulting constraints on the relation between the subhalo mass and various quantities obtained from the multiple data set would provide additional conditions for the comprehensive understanding of the physics of galaxy formation.

The author would like to thank Naoki Yoshida for helpful discussions and comments on the manuscript. We appreciate the helpful comments of the referee. The author is supported by Research Fellowships of the Japan Society for the Promotion of Science (JSPS) for Young Scientists. Numerical calculations for the present work have been in part carried out under the “Interdisciplinary Computational Science Program” in the Center for Computational Sciences, University Tsukuba, and also on the general-purpose PC farm at the Center for Computational Astrophysics, CfCA, of the National Astronomical Observatory of Japan.

REFERENCES

- Baltz, E. A., Marshall, P., & Oguri, M. 2009, *J. Cosmology Astropart. Phys.*, 1, 15
- Brainerd, T. G., Blandford, R. D., & Smail, I. 1996, *ApJ*, 466, 623
- Broadhurst, T., Takada, M., Umetsu, K., et al. 2005, *ApJ*, 619, L143
- Bullock, J. S., Kolatt, T. S., Sigad, Y., et al. 2001, *MNRAS*, 321, 559
- Covone, G., Sereno, M., Kilbinger, M., & Cardone, V. F. 2014, *ApJ*, 784, L25
- Crocce, M., Pueblas, S., & Scoccimarro, R. 2006, *MNRAS*, 373, 369
- Du, W., & Fan, Z. 2014, *ApJ*, 785, 57
- Duffy, A. R., Schaye, J., Kay, S. T., & Dalla Vecchia, C. 2008, *MNRAS*, 390, L64
- Dutton, A. A., Conroy, C., van den Bosch, F. C., Prada, F., & More, S. 2010, *MNRAS*, 407, 2
- Erben, T., Hildebrandt, H., Miller, L., et al. 2013, *MNRAS*, 433, 2545
- Gao, L., White, S. D. M., Jenkins, A., Stoehr, F., & Springel, V. 2004, *MNRAS*, 355, 819
- Gillis, B. R., Hudson, M. J., Erben, T., et al. 2013, *MNRAS*, 431, 1439
- Guzik, J., & Seljak, U. 2002, *MNRAS*, 335, 311
- Hamana, T., & Mellier, Y. 2001, *MNRAS*, 327, 169
- Hamana, T., Miyazaki, S., Kashikawa, N., et al. 2009, *PASJ*, 61, 833
- Hamana, T., Oguri, M., Shirasaki, M., & Sato, M. 2012, *MNRAS*, 425, 2287
- Hamana, T., Takada, M., & Yoshida, N. 2004, *MNRAS*, 350, 893
- Hayashi, E., Navarro, J. F., Taylor, J. E., Stadel, J., & Quinn, T. 2003, *ApJ*, 584, 541
- Hennawi, J. F., & Spergel, D. N. 2005, *ApJ*, 624, 59
- Hilbert, S., & White, S. D. M. 2010, *MNRAS*, 404, 486
- Hinshaw, G., Larson, D., Komatsu, E., et al. 2013, *ApJS*, 208, 19
- Hoekstra, H., Yee, H. K. C., & Gladders, M. D. 2004, *ApJ*, 606, 67
- Hu, W., & Kravtsov, A. V. 2003, *ApJ*, 584, 702
- Hudson, M. J., Gwyn, S. D. J., Dahle, H., & Kaiser, N. 1998, *ApJ*, 503, 531
- Johnston, D. E., Sheldon, E. S., Wechsler, R. H., et al. 2007, *ArXiv e-prints*

- Kneib, J.-P., & Natarajan, P. 2011, *A&A Rev.*, 19, 47
- Komatsu, E., Smith, K. M., Dunkley, J., et al. 2011, *ApJS*, 192, 18
- Leauthaud, A., Tinker, J., Bundy, K., et al. 2012, *ApJ*, 744, 159
- Lewis, A., Challinor, A., & Lasenby, A. 2000, *Astrophys. J.*, 538, 473
- Li, R., Mo, H. J., Fan, Z., Yang, X., & Bosch, F. C. v. d. 2013, *MNRAS*, 430, 3359
- Li, R., Shan, H., Mo, H., et al. 2014, *MNRAS*, 438, 2864
- Mandelbaum, R., Seljak, U., Cool, R. J., et al. 2006a, *MNRAS*, 372, 758
- Mandelbaum, R., Seljak, U., Kauffmann, G., Hirata, C. M., & Brinkmann, J. 2006b, *MNRAS*, 368, 715
- Maturi, M., Meneghetti, M., Bartelmann, M., Dolag, K., & Moscardini, L. 2005, *A&A*, 442, 851
- Ménard, B., Scranton, R., Fukugita, M., & Richards, G. 2010, *MNRAS*, 405, 1025
- Navarro, J. F., Frenk, C. S., & White, S. D. M. 1997, *ApJ*, 490, 493
- Nishimichi, T., Shirata, A., Taruya, A., et al. 2009, *PASJ*, 61, 321
- Oguri, M., Bayliss, M. B., Dahle, H., et al. 2012, *MNRAS*, 420, 3213
- Oguri, M., & Hamana, T. 2011, *MNRAS*, 414, 1851
- Oguri, M., & Takada, M. 2011, *Phys. Rev. D*, 83, 023008
- Okabe, N., Futamase, T., Kajisawa, M., & Kuroshima, R. 2014, *ApJ*, 784, 90
- Okabe, N., Smith, G. P., Umetsu, K., Takada, M., & Futamase, T. 2013, *ApJ*, 769, L35
- Reid, B. A., Percival, W. J., Eisenstein, D. J., et al. 2010, *MNRAS*, 404, 60
- Reyes, R., Mandelbaum, R., Gunn, J. E., et al. 2012, *MNRAS*, 425, 2610
- Reyes, R., Mandelbaum, R., Hirata, C., Bahcall, N., & Seljak, U. 2008, *MNRAS*, 390, 1157
- Sato, M., Hamana, T., Takahashi, R., et al. 2009, *ApJ*, 701, 945
- Seljak, U. 2002, *MNRAS*, 334, 797
- Shirasaki, M., & Yoshida, N. 2014, *ApJ*, 786, 43
- Springel, V. 2005, *MNRAS*, 364, 1105
- Springel, V., White, S. D. M., Tormen, G., & Kauffmann, G. 2001, *MNRAS*, 328, 726

- Tegmark, M., Eisenstein, D. J., Strauss, M. A., et al. 2006, *Phys. Rev. D*, 74, 123507
- Tinker, J., Kravtsov, A. V., Klypin, A., et al. 2008, *ApJ*, 688, 709
- Tinker, J. L., Robertson, B. E., Kravtsov, A. V., et al. 2010, *ApJ*, 724, 878
- Tormen, G., Diaferio, A., & Syer, D. 1998, *MNRAS*, 299, 728
- Valageas, P., & Nishimichi, T. 2011, *A&A*, 527, A87
- Velander, M., van Uitert, E., Hoekstra, H., et al. 2014, *MNRAS*, 437, 2111
- White, M., & Hu, W. 2000, *ApJ*, 537, 1
- Yang, X., Mo, H. J., van den Bosch, F. C., & Jing, Y. P. 2005, *MNRAS*, 356, 1293
- Yang, X., Mo, H. J., van den Bosch, F. C., et al. 2006, *MNRAS*, 373, 1159
- . 2007, *ApJ*, 671, 153

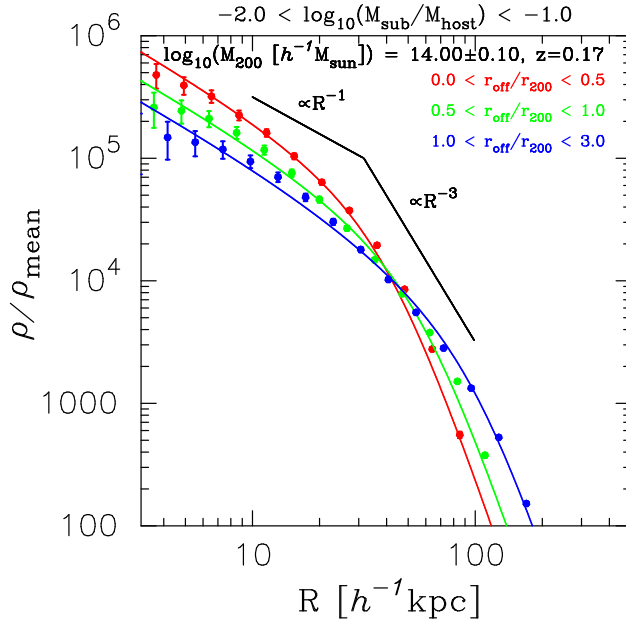


Fig. 8.— Density profile of subhalos as a function of the offset length. We normalize the density profile by the mean matter density. In this figure we show the average density profile of subhalos with the mass of $M_{\text{sub}}/M_{\text{host}} = 0.01 - 0.1$ at $z = 0.17$. We consider the sample of host halos with the mass of $M_{200} = 10^{14 \pm 0.1} h^{-1} M_{\odot}$. Each color point represents the average density profile over subhalos in our N -body simulation. The red point shows the subhalo density profiles at a position with the offset of $r_{\text{off}} = 0.25 \pm 0.25 r_{200}$, the green point is the same for the offset of $r_{\text{off}} = 0.75 \pm 0.25 r_{200}$, and the blue point is the farthest case with $r_{\text{off}} = 2.0 \pm 1.0 r_{200}$. Each color line shows the fitting result with a functional form of the density profile described by Equation (17). The error bar represents the Poisson error within each bin.

A. RADIAL DEPENDENCE OF SUBHALO DENSITY PROFILE IN CLUSTER REGION

In this Appendix, we show the dark matter density profile around subhalos in a high-density region as a function of the offset length with respect to the center of host halo.

We consider the sample of host halos with the mass of $\log(M_{200}/h^{-1} M_{\odot}) = 14.0 \pm 0.1$, which is the typical mass of galaxy cluster. In this binning of M_{200} , we find $\sim 90 - 130$ dark matter halos over the redshift range of $0.1 - 0.3$ in our N -body simulation. For each halo, we select subhalos identified by SUBFIND (Springel et al. 2001) as a function of the offset length from the center of the host halo. We here define the position of the most bound particle in each halo as the center of the host halo. We consider the three subgroups with the offset length of $r_{\text{off}} = 0.25 \pm 0.25 r_{200}$, $0.75 \pm 0.25 r_{200}$ and $r_{\text{off}} = 2.0 \pm 1.0 r_{200}$. In this analysis, we consider the subhalos with $M_{\text{sub}}/M_{\text{host}} = 0.01 - 0.1$, corresponding to $\sim 1000 - 10,000$ particles. In the calculation of the density profile, we bin the radii

$z = 0.10$	N_{sub}	$\ln(\rho_s/\bar{\rho}_m)$	$r_s [h^{-1}\text{kpc}]$	$r_t [h^{-1}\text{kpc}]$
$r_{\text{off}} = 0.25 \pm 0.25 r_{200}$	22	11.4	36.8	38.5
$r_{\text{off}} = 0.75 \pm 0.25 r_{200}$	67	9.45	114.5	63.4
$r_{\text{off}} = 2.0 \pm 1.0 r_{200}$	128	9.61	77.2	108.8
$z = 0.17$	N_{sub}	$\ln(\rho_s/\bar{\rho}_m)$	$r_s [h^{-1}\text{kpc}]$	$r_t [h^{-1}\text{kpc}]$
$r_{\text{off}} = 0.25 \pm 0.25 r_{200}$	18	10.6	63.2	40.2
$r_{\text{off}} = 0.75 \pm 0.25 r_{200}$	61	9.79	81.3	58.1
$r_{\text{off}} = 2.0 \pm 1.0 r_{200}$	155	9.24	93.5	104.0
$z = 0.25$	N_{sub}	$\ln(\rho_s/\bar{\rho}_m)$	$r_s [h^{-1}\text{kpc}]$	$r_t [h^{-1}\text{kpc}]$
$r_{\text{off}} = 0.25 \pm 0.25 r_{200}$	24	11.3	32.9	37.5
$r_{\text{off}} = 0.75 \pm 0.25 r_{200}$	58	9.50	89.9	54.4
$r_{\text{off}} = 2.0 \pm 1.0 r_{200}$	131	9.46	73.0	114.3
$z = 0.32$	N_{sub}	$\ln(\rho_s/\bar{\rho}_m)$	$r_s [h^{-1}\text{kpc}]$	$r_t [h^{-1}\text{kpc}]$
$r_{\text{off}} = 0.25 \pm 0.25 r_{200}$	13	10.5	50.5	39.8
$r_{\text{off}} = 0.75 \pm 0.25 r_{200}$	45	9.33	88.6	56.4
$r_{\text{off}} = 2.0 \pm 1.0 r_{200}$	98	9.27	74.2	109.6

Table 3: The fitting result of subhalo density profile parameters. We use the host halos with the mass of $M_{200} = 10^{14} h^{-1} M_{\odot}$. N_{sub} is the number of subhalos used in the analysis. ρ_s is the scale density, r_s is the scale radius, and r_t represents the effective tidal radius.

from the center of mass of each subhalo logarithmically with the bin size of $\Delta \log(R/R_{\text{far}})=0.2$, where R is the radii from the center and R_{far} is the farthest radii from the center in each subhalo. We then obtain the average density profile of the subhalo as a function of the position in the cluster region.

Figure 8 shows the average density profile around the subhalos. Each color point shows the average profile obtained from our N -body simulation. The red, green and blue points represent the case of subhalos with the offset length of $r_{\text{off}} = 0.25 \pm 0.25 r_{200}$, $0.75 \pm 0.25 r_{200}$ and $r_{\text{off}} = 2.0 \pm 1.0 r_{200}$, respectively. We clearly find the radial dependence of subhalo density profile in the cluster region. This feature is found in the redshift range of 0.1 – 0.3 and the overall shape of density profile is well described by Equation (17), which has the slope of r^{-6} in the outskirts. We fit the average density profile with a functional form of Equation (17). We then find the general trend of the effective tidal radius parameter r_t , (i.e., subhalos have the larger r_t as separating from the center of host halos). The result is summarized in Table 3.